Karazin Kharkiv National University
Department of Physics and Technology

Technische Universität Darmstadt
Institut für Kernphysik

Investigation of the Two - Phonon Quadrupole - Octupole 1^- state in ^{112}Sn with Nuclear Resonance Fluorescence

Diploma Thesis

Inna Pysmenetska

Darmstadt

February 2004

Dedicated to Oleksiy Burda

Contents

Abstract

A systematic study of the spherical semi-magic ^{116,118,120,122,124}Sn nuclei with nuclear resonance fluorescence at excitation energies up to 4 MeV has been performed before. To extend this systematics an investigation of the rare ^{112}Sn isotope was carried out at the Stuttgart Dynamitron facility in the summer of 2003 with a bremsstrahlung end-point energy of 3.8 MeV. In the measured spectra excitation of the first 2^+ state and a dipole state, which is interpreted as the 1^- the member of the $2^+ \otimes 3^-$ two-phonon multiplet, were observed.

A value for the B(E1) transition strength to the ground state and an upper limit for the transition to the 2^+_1 state, which exhibits characteristic features of two-phonon states, are extracted from the data. While the observed excitation energy of the 1^- state fits well into the systematics of the even-mass tin isotopes, the ground-state transition strength was found to be significantly larger.

1 Introduction

In spherical nuclei close to the magic proton or neutron shells the lowest collective excitations are quadrupole and octupole vibrations of the nuclear shape. A coupling of these two single "phonon" excitations leads to a two-phonon quintuplet [1–3] with spins $J^\pi = 1^- \ldots 5^-$. A schematic representation of the shape vibrations and their assumed coupling is displayed in Fig. 1.1. Investigation of two-phonon states gives insight into harmonicity of the vibrational coupling. The 1^- member of this multiplet can in principle be excited via an electric dipole transition from the ground state in nuclear resonance fluorescence experiments. Nuclear Resonance Fluorescence (NRF) is by far the most sensitive tool to detect such dipole excitations and to determine their characteristics.

Nuclear Resonance Fluorescence in general represents an appropriate tool to investigate excitations of low multipolarity in atomic nuclei below the particle threshold [4–6]. In NRF experiments one usually uses bremsstrahlung which is produced by slowing down relativistic electrons. The resulting bremsstrahlung spectrum is continuous in the energy region from zero to the end-point energy which is equal to the incident electron energy. Thus, it allows the simultaneous investigation of nuclear excitations in a wide energy range. Another principal advantage of this method is that both the excitation and deexcitation processes take place via the best understood interaction in physics, the electromagnetic interaction.

In the case of even-even nuclei, a complete set of spectroscopic information can be determined in a model-independent way:

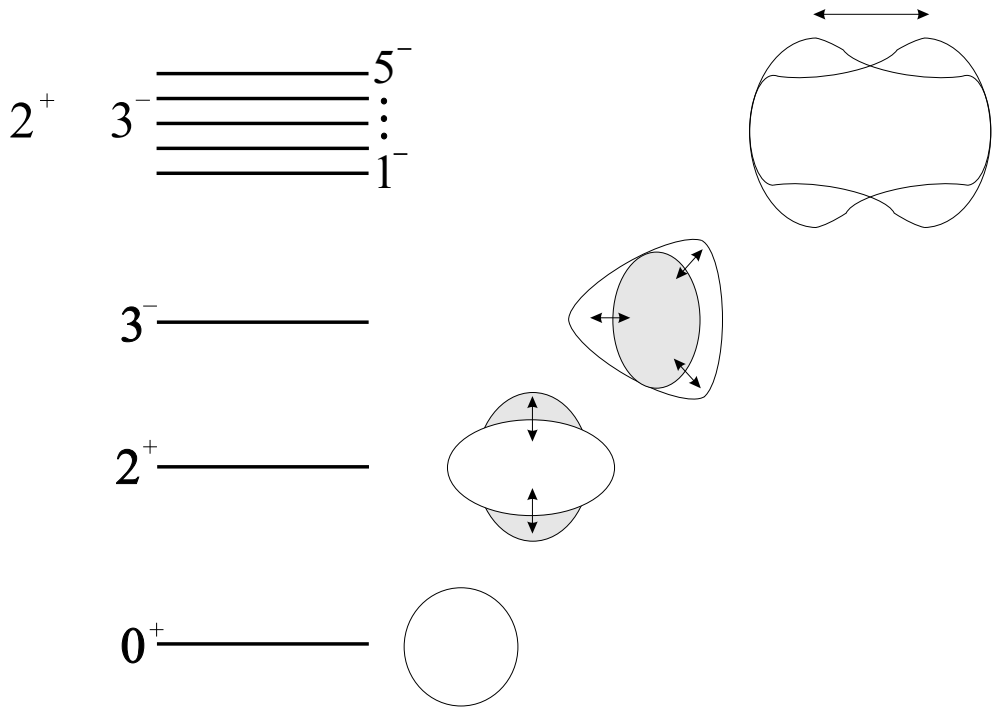

Figure 1.1: Schematic representation of quadrupole (2^+) and octupole (3^-) vibrations and their coupling to two-phonon ($1^- \ldots 5^-$) states.

- level excitation energy E_x,
- total cross section I_S,
- spin J,
- parity π,
- transition width ratio Γ_0^2/Γ,
- $B(\Pi\lambda) \uparrow$ excitation probabilities.

The properties of the $(2^+ \otimes 3^-|1^- >$ state near shell closures have been

investigated in a wide range of nuclei [7, 8].

The even semi-magic Sn isotope nuclei represent an interesting case to investigate the two-phonon quadrupole-octupole coupling. A systematic study of even-mass Sn isotopes with mass numbers 116 up to 124 has been recently reported [9, 10]. To continue the study of even Sn isotopes a NRF experiment on ^{112}Sn was carried out at the 4.3 MV Dynamitron Accelerator of the Stuttgart University. Because of the low natural abundance, data on excited states in ^{112}Sn are scarce [11].

The motivation of the experiment was a detailed characterization of the quadrupole-octupole two-phonon 1^- state in ^{112}Sn with high sensitivity. It allows to extend the systematics to a more proton-rich nucleus and to test whether the reasonable constancy [9] of their properties (excitation energy, B(E1) strength) remains. The Stuttgart Dynamitron facility is an ideal accelerator to investigate transitions to dipole states with excitation energy below 4 MeV.

This thesis is divided into six chapters. A description of the nuclear resonance fluorescence technique is presented in the Chapter 2. Chapter 3 covers details of experimental setup and performance. The analysis and results are summarized in Chapter 4. Chapter 5 presents the discussion of the results. A conclusion is given in Chapter 6.

2 Nuclear Resonance Fluorescence

Nuclear Resonance Fluorescence represents the process of resonant excitation of a nuclear level due to the absorption of a real photon and the subsequent decay of this level by reemission of a photon [4,6]. Figure 2.1 shows a scheme of excitation and decay in the nucleus. A nucleus with the spin J_0 and parity π_0 absorbs a real photon and is left in an excited level with energy E_x, spin J and parity π. After some time (typically fs to ps) the excited nuclei will decay back to the ground state (elastic transition) or to some other low-lying excited state with the energy E_i, angular momentum J_i, and parity π_i (inelastic transition).

The quantities Γ_0, Γ_i, and Γ denote the transition widths to the ground state, to an intermediate level, and the total transition width, respectively. The correspondence between the widths is

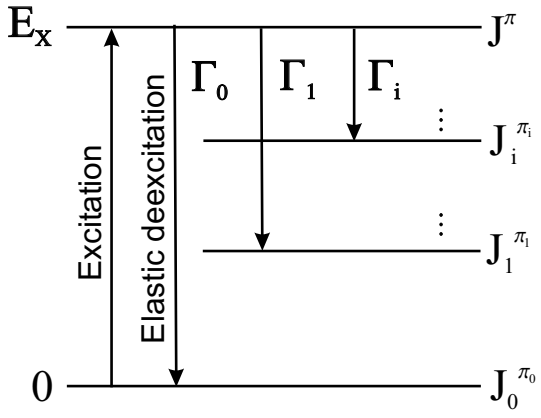

Figure 2.1: Gamma-ray transitions in nuclear resonance fluorescence.

$$\Gamma = \Gamma_0 + \sum_{i>0} \Gamma_i, \tag{2.1}$$

with i being the sum over all intermediate levels. The total decay width and the lifetime τ of a level are connected via the Heisenberg uncertainty relation

$$\tau \cdot \Gamma = \hbar. \tag{2.2}$$

Furthermore, the partial widths define the branching ratios

$$b_0 = \frac{\Gamma_0}{\Gamma}. \tag{2.3}$$

and

$$b_i = \frac{\Gamma_i}{\Gamma}. \tag{2.4}$$

2.1 Scattering Cross Sections

The cross section for the process of a nuclear transition from the ground state through an excited state to a final state is described by the Breit-Wigner formula

$$\sigma^i_{abs}(E_\gamma) = \frac{\pi}{2} \cdot \left(\frac{\hbar c}{E_x}\right)^2 \cdot g \cdot \frac{\Gamma_0 \Gamma_i}{(E_\gamma - E_x)^2 + \frac{\Gamma^2}{4}}, \tag{2.5}$$

where E_x is the excitation energy, E_γ is the energy of the incoming photon, and g is a statistical factor, which depends upon the ground state total angular momentum J_0 and the angular momentum of the excited level J

$$g = \frac{2J+1}{2J_0+1}. \tag{2.6}$$

The total cross section is given by the sum of partial cross sections of the decays to all possible final states

$$\sigma_{abs}^{total}\left(E_\gamma\right) = \sum_i \sigma_{abs}^i\left(E_\gamma\right) = \frac{\pi}{2} \cdot \left(\frac{\hbar c}{E_x}\right)^2 \cdot g \cdot \frac{\Gamma_0 \Gamma}{\left(E_\gamma - E_x\right)^2 + \frac{\Gamma^2}{4}}. \tag{2.7}$$

Another important factor for NRF experiments is the thermal motion of the atoms in the target. This motion causes a Doppler broadening of the line width. It can be assumed that the thermal velocities of nuclei v have a Maxwellian distribution

$$f\left(v\right) = \left(\frac{M}{2\pi kT}\right)^{\frac{1}{2}} \exp\left(-\frac{Mv^2}{2kT}\right), \tag{2.8}$$

where M is the nuclear mass, k is the Bolzmann constant, and T the absolute temperature.

Then, instead of Eq. (2.5), we obtain the Doppler-broadened Breit-Wigner distribution [4, 12]

$$\sigma_{DBW}^i\left(E_\gamma, T\right) = 2\pi \cdot \left(\frac{\hbar c}{E_x}\right)^2 \cdot g \cdot \frac{\Gamma_0}{\Gamma} \cdot \frac{\Gamma_i \sqrt{\pi}}{2\Delta} \exp\left[-\left(\frac{E_\gamma - E_x}{\Delta}\right)^2\right], \tag{2.9}$$

where Δ is the Doppler width

$$\Delta = E\sqrt{\frac{2k_B T}{Mc^2}}. \tag{2.10}$$

This Doppler-broadened distribution can be used to deduce immediately the total elastic scattering cross section I_s integrated over a single resonance and over the complete solid angle from Eq. (2.9)

$$I_i = \int \sigma^i_{DBW}\left(E_\gamma, T\right) dE_\gamma = \pi^2 \cdot \left(\frac{\hbar c}{E_x}\right)^2 \cdot g \cdot \frac{\Gamma_0 \Gamma_i}{\Gamma}. \tag{2.11}$$

In the case of an elastic transition ($\Gamma_i = \Gamma_0$) we have

$$I_0 = \pi^2 \cdot \left(\frac{\hbar c}{E_x}\right)^2 \cdot g \cdot \frac{\Gamma_0^2}{\Gamma}. \tag{2.12}$$

2.2 Reduced Transition Probabilities

The electromagnetic transitions are characterized by the multipole order λ with $\lambda = 1, 2, ...$ for dipole, quadrupole, ... transitions. There exists a selection rule for allowed electromagnetic transitions relating the total angular momenta of the initial and final states J_i and J_f with the multipolarity of the transition from these two states

$$|J_i - J_f| \leq \lambda \leq J_i + J_f. \tag{2.13}$$

The multipole character is defined by the parities of these states

$$\pi_i = (-1)^\lambda \cdot \pi_f \qquad \text{for electric transitions,} \tag{2.14}$$

$$\pi_i = (-1)^{\lambda+1} \cdot \pi_f \qquad \text{for magnetic transitions.} \tag{2.15}$$

The decay width [6] into the ground state Γ_0 is proportional to the reduced transition probability $B(\Pi\lambda, E_\gamma)\uparrow$

$$\Gamma_0 = 8\pi \sum_{\Pi\lambda=1}^{\infty} \frac{(\lambda+1)}{\lambda\left[(2\lambda+1)!!\right]^2} \cdot \left(\frac{E_\gamma}{\hbar c}\right)^{2\lambda+1} \cdot \frac{2J_0+1}{2J+1} \cdot B\left(\Pi\lambda, E_\gamma\right)\uparrow \qquad (2.16)$$

where $\Pi = E$ for electric transitions and $\Pi = M$ for magnetic transitions. The photon can transfer only a small angular momentum to a nucleus. Therefore in NRF experiments mostly dipole transitions and to a lesser extent electric quadrupole transitions ere exciteed.

The reduced transition probabilities for the decay $B\left(\Pi\lambda; J \to J_0\right) = B\left(\Pi\lambda\right)\downarrow$ and excitation $B\left(\Pi\lambda; J_0 \to J\right) = B\left(\Pi\lambda\right)\uparrow$ differ by the statistical factor introduced in Eq. (2.6)

$$B\left(\Pi\lambda\right)\uparrow = \frac{2J+1}{2J_0+1} \cdot B\left(\Pi\lambda\right)\downarrow . \qquad (2.17)$$

For even-even nuclei one has the following relations between reduced transition strength and the ground state decay width

$$\frac{B\left(E1\right)\uparrow}{[\mathrm{e}^2\mathrm{fm}^2]} = 9.554 \cdot 10^{-4} \cdot g \cdot \frac{\Gamma_0}{[\mathrm{meV}]} \cdot \left(\frac{[\mathrm{MeV}]}{E_x}\right)^3 , \qquad (2.18)$$

$$\frac{B\left(M1\right)\uparrow}{[\mu_\mathrm{N}^2]} = 8.641 \cdot 10^{-2} \cdot g \cdot \frac{\Gamma_0}{[\mathrm{meV}]} \cdot \left(\frac{[\mathrm{MeV}]}{E_x}\right)^3 , \qquad (2.19)$$

$$\frac{B\left(E2\right)\uparrow}{[\mathrm{e}^2\mathrm{fm}^4]} = 1.245 \cdot 10^{3} \cdot g \cdot \frac{\Gamma_0}{[\mathrm{meV}]} \cdot \left(\frac{[\mathrm{MeV}]}{E_x}\right)^5 . \qquad (2.20)$$

2.3 Angular Distributions

By measuring the angular distribution of the emitted photons with respect to the incident beam in the NRF experiments, the multipole order (dipole or quadrupole) of a transition can be determined [6]. The angular distribution function $W(\theta)$ for resonantly scattered real photons is given by the following expression [13]

$$W(\theta) = \sum_{\nu=0,2,4,\ldots} A_\nu^{i\to j} \cdot A_\nu^{j\to k} P_\nu(\cos\theta), \tag{2.21}$$

with θ being the scattering angle between the direction of the incident photon and the scattered photon and $P(\cos\theta)$ the Legendre polynomials. The coefficient $A_\nu^{i\to j}$ describes the photon in the entrance channel, and similarly $A_\nu^{j\to k}$ takes into account the resonantly scattered photon.

Nuclei with even proton and neutron numbers always have a ground state angular momentum and parity $J_0^\pi = 0^+$. As a consequence, only levels with spin 1 or 2 can be excited in (γ,γ') measurements. In the case of elastic scattering, only the spin sequences $0-1-0$ and $0-2-0$ will occur, corresponding to pure dipole and quadrupole transitions, and the following expressions for the angular distribution functions $W(\theta)$ are obtained [14]

$$W(\theta)_{0\to1\to0} = \frac{3}{4}\cdot\left(1+\cos^2\theta\right), \tag{2.22}$$

$$W(\theta)_{0\to2\to0} = \frac{5}{4}\cdot\left(1-3\cos^2\theta+4\cos^4\theta\right). \tag{2.23}$$

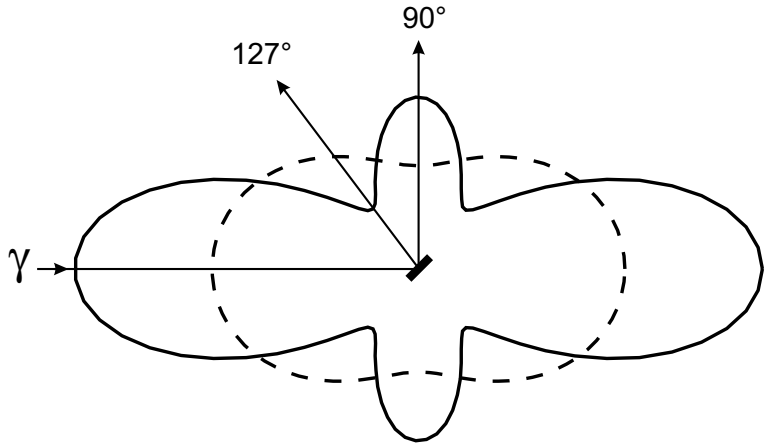

Figure 2.2: Radial plot of the angular distribution functions for pure dipole ($W(\theta)_{0\to1\to0}$, dashed curve) and quadrupole ($W(\theta)_{0\to2\to0}$, solid curve) elastic transitions in even-even nuclei.

These angular distribution functions are plotted in Fig. 2.2. From this figure one can see that at 90° the angular distribution for dipole transitions has a minimum whereas for quadrupole transitions it has a maximum at 90° and two minima at 53° and 127°. The angle 127° is more favorable than 53° for a NRF experiment due to the dramatic background decrease at backward angles (because of the dominance of atomic scattering at forward angles), so the best distinction between the two distributions exists at the scattering angles of 90° and 127°. Thus, in the case of an even-even nucleus, measurements of the γ intensities at two angles (90° and 127°) allow the determination of the multipole order λ and thus the angular momentum J of the excited level. The ratio of the measured scattered γ intensities at 90° and 127° should result in one of the two expected values

$$\frac{W(90^\circ)_{0\to1\to0}}{W(127^\circ)_{0\to1\to0}} = 0.73 \qquad \text{or} \qquad \frac{W(90^\circ)_{0\to2\to0}}{W(127^\circ)_{0\to2\to0}} = 2.28 \tag{2.24}$$

There may be a difference between the theoretical values and the experimental ones because of the finite opening angles of the detectors and feeding of the low-lying levels from the higher lying excited states.

3 Experimental Procedures

3.1 Dynamitron Accelerator and Experimental Facilities

The Nuclear Resonance Fluorescence experiment was performed at the cascade Dynamitron accelerator of the Stuttgart University [15, 16]. The Dynamitron (see Fig. 3.1) is a single-ended electrostatic generator which can be used to accelerate electrons as well as positively charged ions. The maximum electron current which can be achieved is 4 mA with a maximum energy of 4.3 MeV.

To avoid scattering of accelerated particles with gas molecules, the accelerator tube and the beam transport system are evacuated to a vacuum of $10^{-6} - 10^{-7}$ mbar.

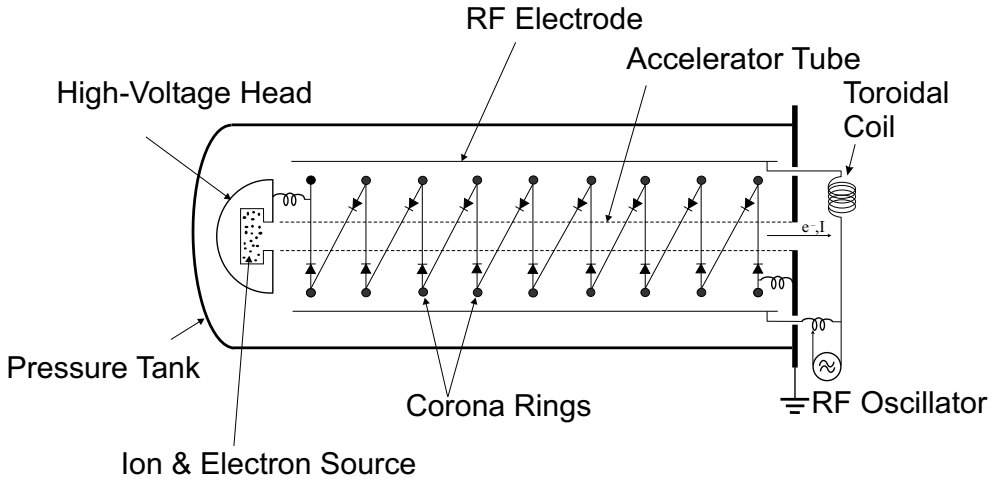

Figure 3.1: Schematic layout of the Dynamitron.

The electrons are generated by heating a filament. A voltage gradient causes the electrons to be extracted from the area surrounding the filament. The electrons are then accelerated and collimated as they travel through the beam tube. The electrodes and corona rings play the role of capacitors. The two electrodes and the coil form an electrical circuit which is fed by the radio-frequency oscillator. Thus the electron energy is equal to the product of the electron charge and the total voltage.

In Fig. 3.2 the whole experimental facility consisting of the Dynamitron accelerator, the beam transport system and all setups are depicted. The electron beam delivered from the Dynamitron accelerator can be deflected by an analyzing magnet and guided to the different experimental facilities such as the 120° beam line for photon scattering experiments [17, 18], a 90° beam line, a 60° beam line for experiments in nuclear astrophysics, a 21° beam line for solid state physics, and a 0° beam line.

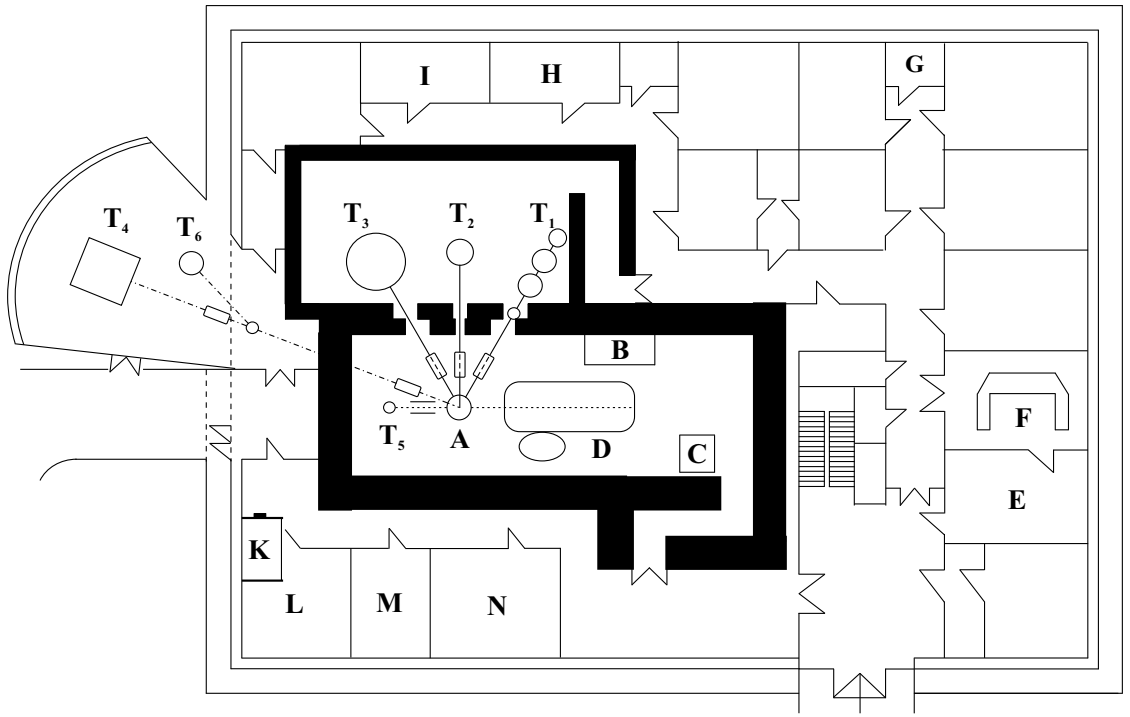

A Analysing magnet
B SF_6 gas system
C Oscillator
D Dynamitron tank
E Counting room
F Control room
G General workstation

H Counting room
I Ethernet server-room
K Technicians
L Technicians
M Technicians
N Technicians
T_1 120^0 target
Photon scattering facility

T_2 90^0 target
T_3 60^0 target
T_4 21^0 target
Windowless gas target
T_5 0^0 target
T_6 Ion beaming and target
station under construction

Figure 3.2: Schematic layout of the Stuttgart Dynamitron Accelerator Laboratory.

3.2 NRF Setup

For NRF experiments the high current DC electron beam is bent by 120° into the beam line at which the NRF setup is placed. Bremsstrahlung is produced in a gold radiator target. It has a thickness of 4 mm in which the electrons are completely stopped. Gold was chosen as basic material for the radiator target because of its high Z value which makes it very efficient for producing bremsstrahlung and because of its good thermal conductivity characteristics. Part of the electron energy is converted into γ-rays, the other part of the energy is converted into heat. Therefore, the radiator target is water cooled with a pressure of 50 bar. The thermal capacity of the gold radiator limits the electron beam current to about 250 μA for 4.1 MeV electrons (typical electron energy in the NRF experiment). In the gold radiator target very intense γ-beams are produced with a flux of typically 10^6 photons/keV/s for 3 MeV photons. Before entering the experimental room, the continuous bremsstrahlung spectrum is hardened by a lead absorber (reducing the intensity of low energy photons) and collimated by a 1 m long lead tube with a diameter of 10 mm.

The experimental area (Fig. 3.3) is separated from the generator room, where the Dynamitron accelerator is located, by a 2 m thick concrete wall. This avoids γ-ray background in the experimental room resulting from the accelerator and the beam transport system. The highly collimated γ-beam enters an evacuated tube (vacuum $10^{-3} - 10^{-4}$ mbar to avoid scattering of the γ-beam off air molecules) which contains the NRF targets under investigation. Due to the high quality of the intense beam, two NRF setups can be oper-

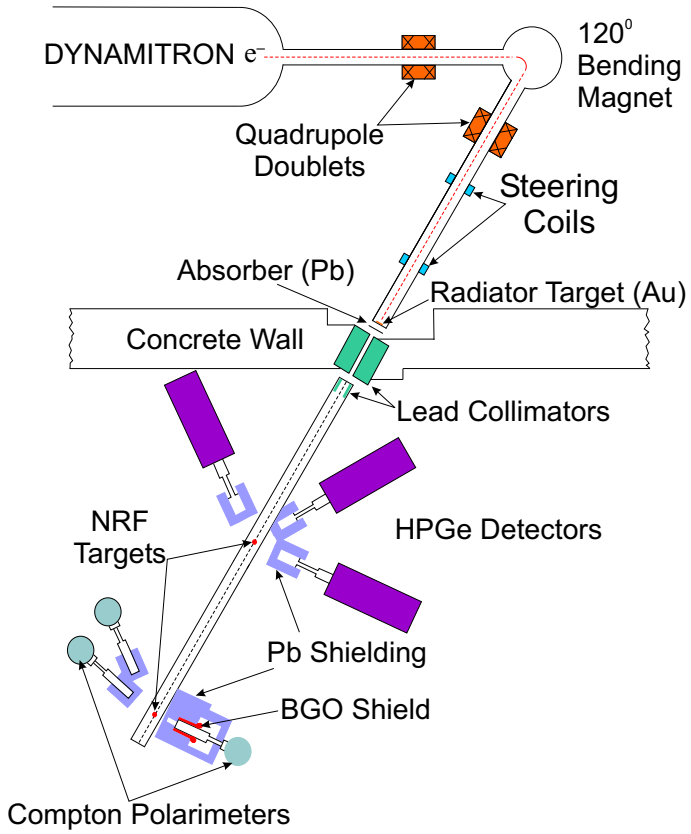

Figure 3.3: Schematic layout of the NRF setup at the Dynamitron.

ated simultaneously. A first setup is used to perform angular distribution and cross section measurements. This setup consist of three HPGe detectors placed at the scattering angles of 90°, 127°, and 150°. Nowadays, large volume HPGe detectors with an efficiency of 100% (relative to a $3'' \times 3''$ NaI(Tl) scintillation crystal) and a good energy resolution of about 2.0 keV at 1.33 MeV (γ-ray produced by the radioactive ^{60}Co nucleus) are available. Typical measuring times at this setup are about 2 days for even-even nuclei and 4 days in the case of odd-mass nuclei. These relatively short measuring

times can be achieved due to high singles counting rates up to 10 kHz per detector [6].

At the second setup a combination of (γ, γ') angular distributions and photon linear polarization measurements is carried out. This setup consists of two Compton polarimeters, placed at slightly backward scattering angles of 95° and an additional HPGe detector located at 127°. The Compton polarimeters are used to determine the linear polarization of the resonantly scattered photons. This enables to deduce the parities of excited levels. Since the signal from the core of the Compton polarimeter carries already the full energy information of the detected rays, angular distribution measurements can be performed simultaneously at this setup. More technical details of the operation of the Compton polarimeters are given in [19, 20]. At this setup only even-even nuclei are studied because it is hardly possible to determine parities of levels in odd-mass nuclei due to the small anisotropy. The accumulation of experimental data with sufficient statistical accuracy for parity determination requires measuring times of 3 to 4 weeks.

In front of each Ge detector or Compton polarimeter a lead filter is placed to reduce the intensity of low energy photons (mainly with energies below 1 MeV). Otherwise, the large flux of these low energy photons can cause pile-up problems in the data acquisition system. The counting rate in the detectors should not exceed 10 kHz. Each Ge detector is surrounded with a lead shield to suppress the background.

All detectors were surrounded by active BGO shields. BGO detectors [21] are based on an inorganic bismuth germanate scintillator ($Bi_4Ge_3O_2$) material

and used to detect photons which have not completely lost their energy in the detector, and also cosmic rays. The large atomic number of Bi (Z=83) and its high density (7.3 g/cm^2) make BGO ideal for the detection of high energy γ-rays.

3.3 Germanium γ-Ray Spectrometers

High-purity Germanium (HPGe) detectors were used in the present experiment. These are semiconductor detectors with very low impurity concentrations of approximately 10^{10} atoms/cm^3, which are much easier to handle than lithium-ion drifted detectors. For instance, they can be warmed to room temperature when they are not in use, while the lithium-ion drifted detectors have to maintained at low temperature at all times. During operation, the HP Ge detectors are cooled with liquid nitrogen to a temperature of 77 K to reduce thermal electronic noise (the band gap in Ge is 0.7 eV only).

In the case of γ-ray spectroscopy at high energies of several MeV, detectors with a large active volume are needed. This can be fulfilled in a cylindrical or coaxial geometry. In this case, one electrode is fabricated at the outer cylindrical surface (see Fig. 3.4) of a long germanium cylindrical crystal, while a second inner cylindrical contact is obtained by removing the core of the crystal. The HP Ge detectors used at the Stuttgart NRF facility have actually a closed-ended coaxial configuration in which only a part of the central core has been removed. The outer electrode covers the cylindrical surface and one flat closed end of the crystal. The electrical properties of the HP Ge crystal depend of the remaining low-level impurities. In the case of

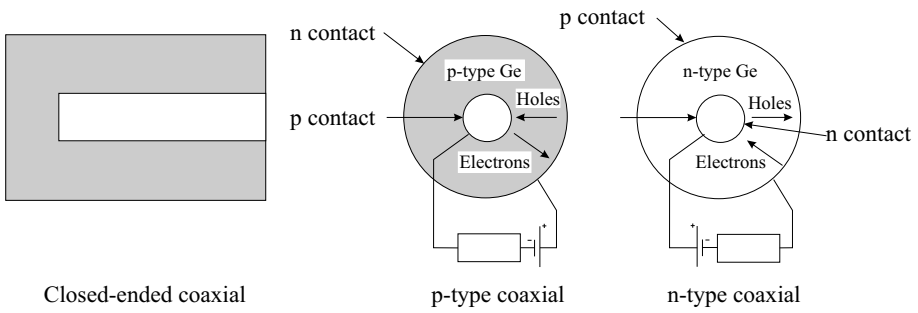

Figure 3.4: Scheme of a closed-ended HP Ge detector.

remaining acceptor impurities, the HP Ge crystal will be p-type (similarly donor impurities give rise to a n-type HP Ge crystal). A positive bias voltage is applied to the n-contact with respect to the p-contact.

The detection of γ-rays critically depends on the number of electron-hole pairs created in the interaction with the detector material. The most important interaction processes of photons with matter are photo-electric absorption, Compton scattering and pair production. In all these processes free electrons are created in the detector material. The energy required to form an electron-hole pair in HPGe detectors is about 3 eV. This means that a large number ($> 10^5$) of electron-hole pairs can be formed, and so many charge carriers are released for each γ-ray interaction. This has two consequences: first, there are small statistical fluctuations in the number of charge carriers per pulse, and second, as a result of the large number there is an excellent signal-to-noise ratio, both resulting to a good energy resolution. The HP Ge detectors are housed in a vacuum-tight cryostat to inhibit thermal conductivity between the crystal and the surrounding air. Secondly, a high voltage is applied to the crystal to saturate the electron and hole drift velocities in

the crystal in order to make the response time of the detector as short as possible and to minimize losses during charge collection.

The most outstanding characteristic of HP Ge detectors is their excellent energy resolution ($< 0.2\%$), allowing the separation of many close-spaced gamma peaks which occur in NRF studies on heavy nuclei or odd-mass nuclei with high level densities. The energy resolution is determined by the statistical spread in the number of charge carriers, variation in the collection efficiency, and the contribution of the electronic noise. Generally, gamma-ray energies can be extracted from the recorded (γ, γ') spectrum with a precision better than 1 keV. More details about radiation detection and the performances of Ge detectors as spectrometers can be found in [21].

3.4 Experimental Details

The experiment was carried out at the Dynamitron accelerator in summer of 2003. Electrons with an energy 3.8 MeV were used to generate bremsstrahlung spectra. The average electron beam current was about 200 μA. The total measurement time was about 69 hours.

The different components of the target are displayed schematically in Fig. 3.5. The target was contained in a poly methyl methacrylate (PMMA) frame ⑤ with kapton foils as front and back sides ④ and made of isotopically-enriched ^{112}Sn material ② . The square ^{112}Sn target was put in front of a ^{27}Al plate ③ with the size 2×2 cm^2. In front of the container isotopically enriched ^{13}C ① was placed in a polyethylene finger. The well-known transitions in ^{27}Al and ^{13}C were used for the energy calibration of the detec-

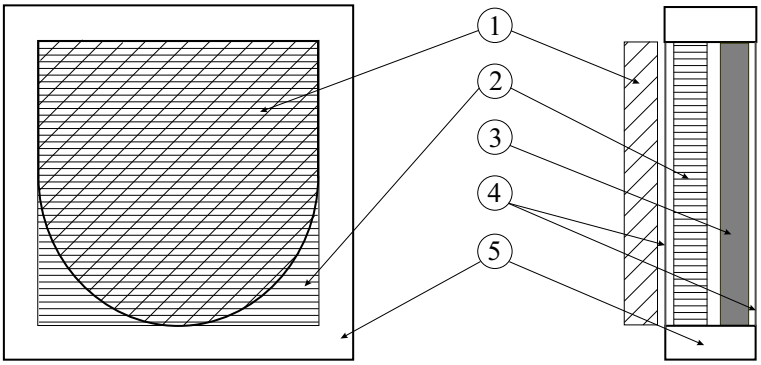

Figure 3.5: Schematic layout of the target. ① polyethylene finger contained ^{13}C, ② ^{112}Sn plate, ③ ^{27}Al plate, ④ poly methyl methacrylate (PMMA) foils, ⑤ container's frame.

tors during the experiment. The masses and abundances are summarized in Table 3.1.

The γ-decay of excited levels was observed with three HPGe detectors of the type described above, which were positioned at 90°, 127° and 150° with respect to the incident beam. Spectra of all 3 detectors were recorded simultaneously by the data acquisition system.

Table 3.1: Masses and abundances of the target .

Element	Mass (g)	Abundance (%)
^{112}Sn	1.99049(5)	99.5
^{27}Al	1.099(1)	100
^{13}C	0.0726(5)	99.0

4 Data Analysis and Results

4.1 Energy Calibration

The well-known transitions in ^{27}Al and ^{13}C were used to determine the energy calibration of the system, i.e., the correspondence between the channels in the data acquisition system and γ-ray energies.

The odd-mass nucleus ^{27}Al is commonly used in NRF experiments to calibrate the photon flux. Integrated cross sections I_S of unknown excited levels in the target under consideration are determined relatively to the various well-known transitions in ^{27}Al. Absolute level widths Γ and lifetimes τ have been determined precisely in nuclear self-absorption experiments on ^{27}Al [22, 23]. These results are summarized in Tab. 4.1, and the deduced total scattering cross sections I_S for the levels in ^{27}Al are given as well.

The odd-mass nucleus ^{13}C has two levels below an excitation energy of 4 MeV which can be used as well for photon flux calibration purposes. Their level widths have been determined in nuclear self-absorption measurements [24,25] and the corresponding results are included in Tab. 4.1.

Energy calibrations for all spectra have been performed. The result of such a calibration for the example of the 90° spectrum is shown in Fig 4.1 with linear function, describing the data very well.

Table 4.1: Excited states of ^{27}Al and ^{13}C including the values of total angular momentum and parity, absolute lifetimes, level widths and deduced total scattering cross sections.

Element	E_x (keV)	J_i^π	τ (fs)	Γ_0/Γ [a] (%)	Γ [b] (meV)	I_S (eV · b)
^{27}Al	2211.1(6) [a]	$7/2^+$	38.1(10) [b]	100 [a]	17.19(31) [b]	18.0(3)
	2734.9(7) [a]	$5/2^+$	14(6) [b]	22.1(10) [a]	51(7) [b]	1.3(2)
	2982.0(1) [a]	$3/2^+$	5.63(13) [b]	97.4(5) [a]	116.7(25) [b]	31.9(8)
	3004.2(8) [a]	$9/2^+$	93(39) [b]	88.6(11) [a]	7.74(46) [b]	4.3(3)
	3956.8(4) [a]	$3/2^+$	3.94(40) [b]	85.3(15) [a]	177(11) [b]	21.1(17)
^{13}C	3089.443(20) [c]	$1/2^+$	1.23(9) [d]	100 [c]	537(42) [d]	216(17)
	3684.507(19) [c]	$3/2^-$	1.63(12) [d]	99(4) [c]	403(30) [d]	224(26)

[a] From Ref. [22].
[b] From Ref. [23].
[c] From Ref. [25].
[d] From Ref. [24].

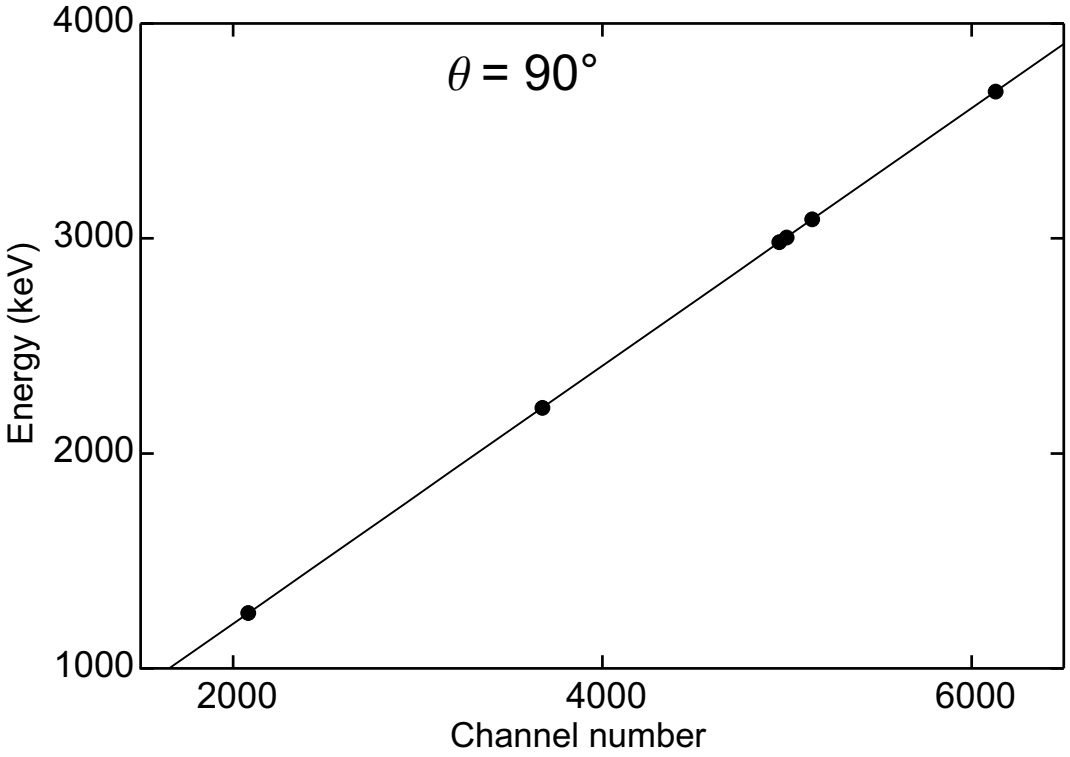

Figure 4.1: Energy calibration of the detector at 90° using known transitions in ^{27}Al and ^{13}C. The data are marked as circles, and the solid line is a linear fit to the data points. The error bars of the data are smaller than the symbols.

Figure 4.2 shows the resulting energy-calibrated experimental (γ, γ') spectrum of ^{112}Sn at θ=90° for the energy region between 1 and 4 MeV in a logarithmic scale. The background due to the nonresonant and atomic scattering decreases approximately exponentially with increasing energy.

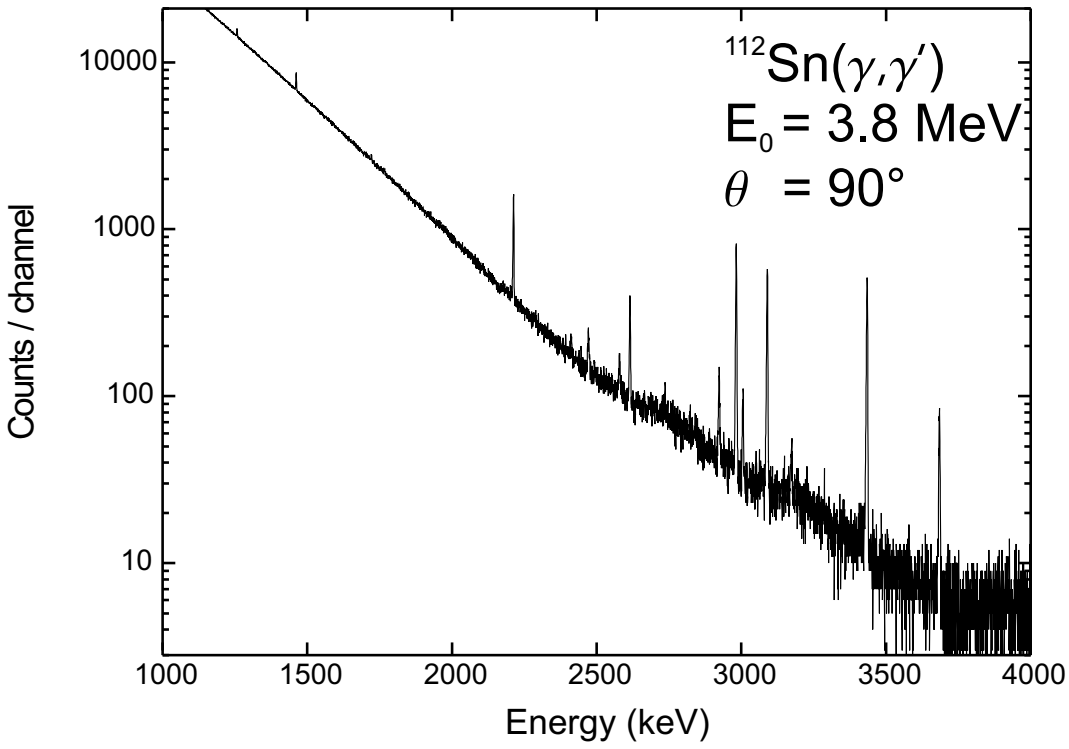

Figure 4.2: Energy-calibrated (γ, γ') spectrum of ^{112}Sn in the energy region from 1 to 4 MeV.

In Fig. 4.3 spectra for all three measured angles are presented in the energy region 1 to 4 MeV. In all spectra we can see the ^{27}Al and ^{13}C calibration lines and their single escape (SE) and double escape (DE) lines, and also a ^{208}Pb background line. One unknown transition, at 3434 keV, and its SE and DE lines are found, which is attributed to ^{112}Sn. Furthermore, excitation of the well-known 2_1^+ state was also observed in the spectra. The relative intensities of lines are different in the spectra because of the angular distributions discussed in Sec. 2.3.

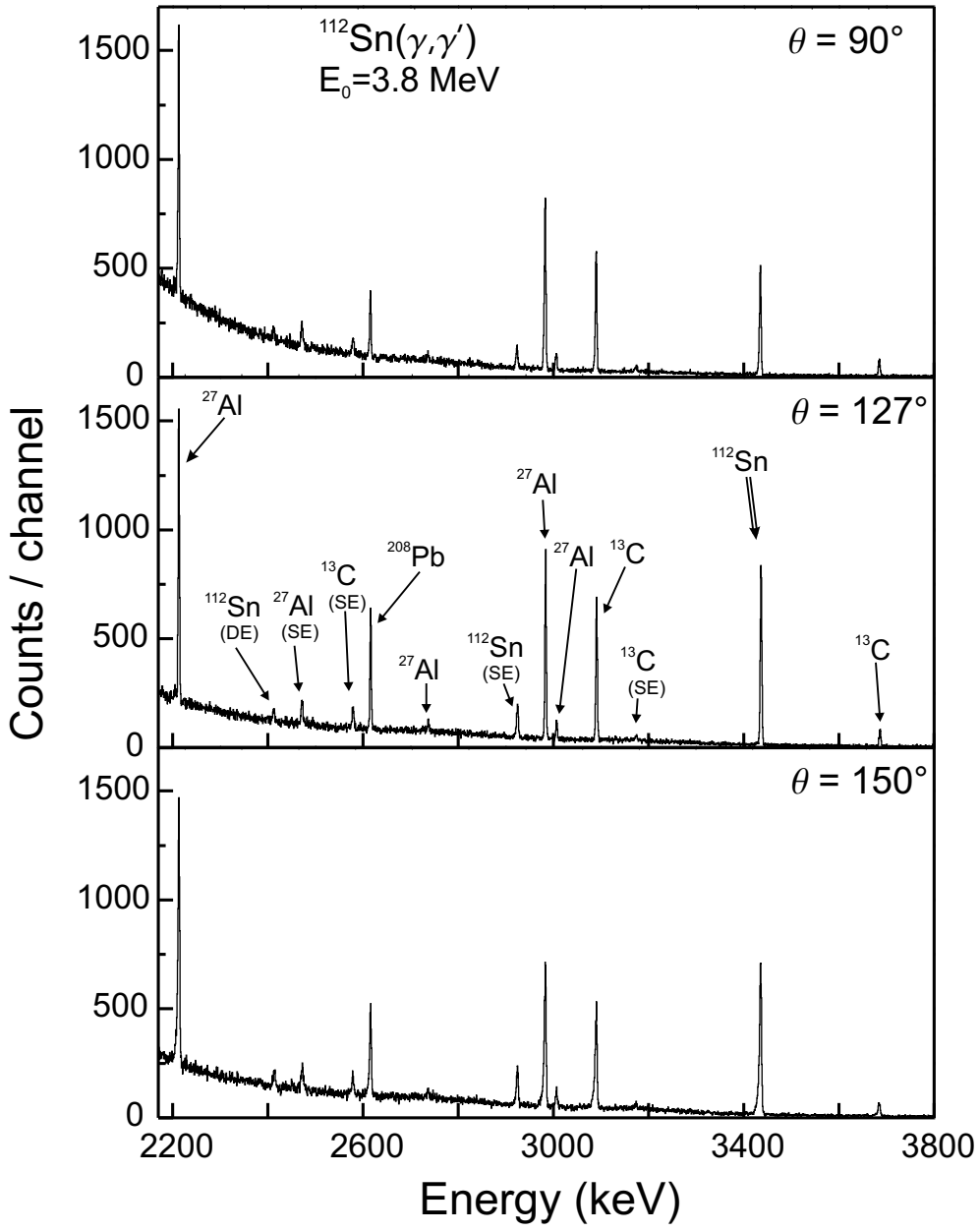

Figure 4.3: Energy calibrated (γ, γ') spectra of ^{112}Sn in the energy region from 2.2 to 3.8 MeV.

4.2 Efficiency Calibration

The energy dependence of the intrinsic efficiency $\varepsilon(E)$ can be determined for each detector from a measurement using a ^{56}Co source. An isotope ^{56}Co is an unstable nucleus, β^+-decaying to ^{56}Fe with a half life of 77.3 days. The radioactive ^{56}Co source provides 19 γ transitions between 0.6 and 3.6 MeV with well known relative γ intensities. In Tab. 4.2 the energies of the emitted γ's are given as well as their relative gamma intensities. Thus, the efficiency can be deduced relatively to the strongest transition at 847 keV by

$$\varepsilon_{Co}(\theta) = \frac{A_{Co}(\theta)}{I_\gamma}, \tag{4.1}$$

with an uncertainty

$$\frac{\Delta(\varepsilon_{Co}(\theta))}{\varepsilon_{Co}(\theta)} = \frac{\Delta(I_\gamma)}{I_\gamma} + \frac{\Delta(A_{Co}(\theta))}{A_{Co}(\theta)}. \tag{4.2}$$

Here $A_{Co}(\theta)$ is the count rate in the respective detector with uncertainty $\Delta(A_{Co}(\theta))$, and I_γ is the appropriate level intensity with uncertainty $\Delta(I_\gamma)$.

The efficiency calibration spectra have been recorded using a ^{56}Co source with the same dimensions as the NRF target that was placed exactly at the target position. This procedure takes into account the solid angle of the detector and the thicknesses of the lead filters in front of detectors [26]. The shape of the relative efficiency curve can be approximated using the empirical formula

$$\varepsilon_{Co}(E) = \frac{a}{E} + b + c \cdot E + d \cdot E^2. \tag{4.3}$$

Table 4.2: Calibration lines of ^{56}Co with their intensities from [11].

Energy (keV)	Intensity %
846.771(4)	99.933(7)
977.373(4)	1.43(14)
1037.840(6)	14.13(5)
1175.102(6)	2.239(11)
1238.282(7)	66.07(19)
1360.215(12)	4.256(15)
1771.351(16)	15.49(5)
1810.772(17)	0.657(20)
1963.714(12)	0.706(10)
2015.181(16)	3.029(13)
2034.755(13)	7.771(27)
2113.123(10)	0.366(6)
2212.933(18)	0.390(7)
2598.459(13)	16.96(6)
3009.596(7)	0.994(21)
3201.962(16)	3.13(3)
3253.416(15)	7.63(24)
3272.990(15)	1.78(6)
3451.152(17)	0.93(4)
3547.930(60)	0.178(9)

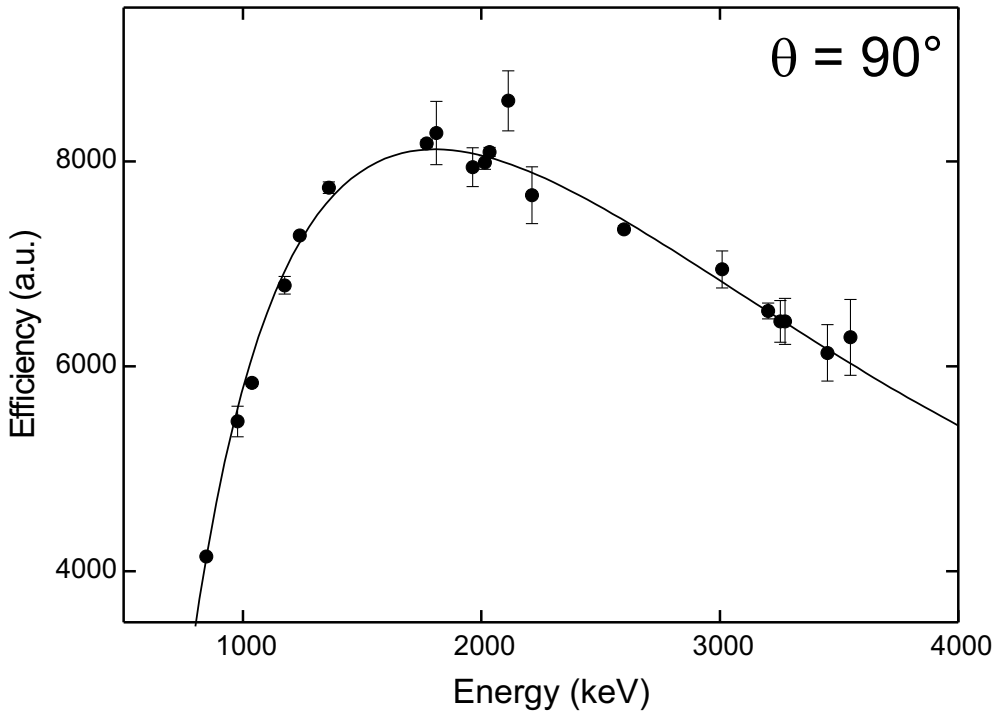

Figure 4.4: Relative efficiency of an HPGe detector, placed at 90°, determined with a radioactive ^{56}Co source at the position of the NRF target.

The measured relative efficiencies and the result of such a fit procedure are shown in Fig. 4.4 for the case of the 90° detector. The efficiency decreases below an energy of about 1.8 MeV due to the influence of the lead absorber placed in front of the detector.

4.3 Experimental Angular Distributions

The multipolarities of the observed transitions can be extracted from the ratio of the peak intensities measured at different scattering angles. Figure

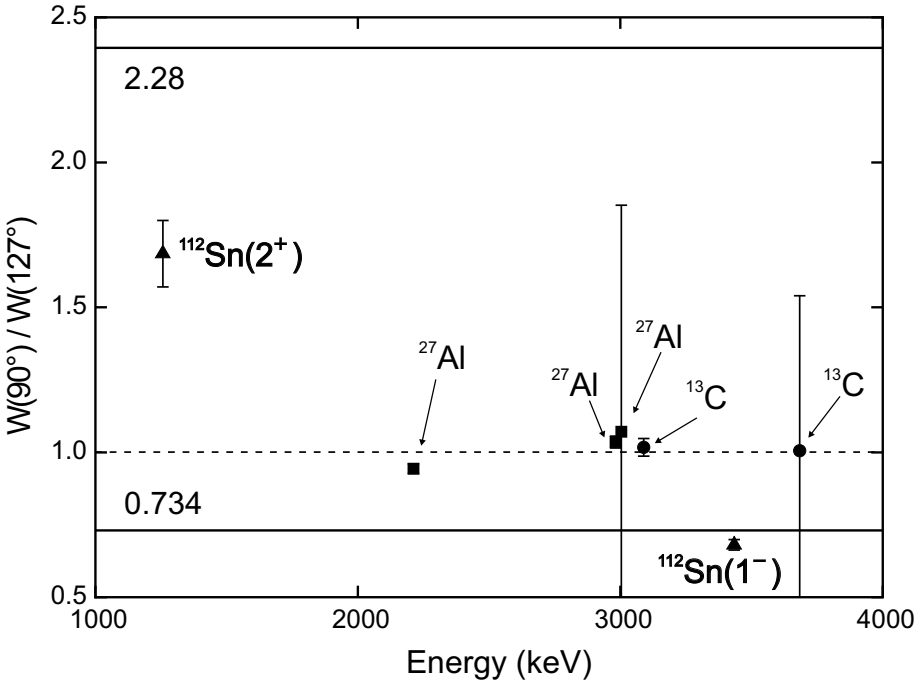

Figure 4.5: Angular distributions of the transitions excited in the ^{112}Sn(γ, γ') reaction at $E_0 = 3.8$ MeV. The triangles belong to ^{112}Sn, and squares and circles to ^{27}Al and ^{13}C, respectively.

4.5 shows these measured ratios at 90° and 127°. The triangles mark levels belonging to ^{112}Sn, and the squares and circles to ^{27}Al and ^{13}C, respectively. The solid lines in this figure represent the theoretically predicted ratios of the angular distribution functions $W(90°)/W(127°)$ for dipole $(0 \rightarrow 1 \rightarrow 0)$ and quadrupole $(0 \rightarrow 2 \rightarrow 0)$ transitions, corrected for the solid angles of the detectors, as well as an isotropic distribution (dashed line).

In the measured spectra we can identify the first 2^+ state of ^{112}Sn at 1257 keV and an unknown excitation at 3435 keV. The extracted value of the intensity

ratio for the first 2^+ state of ^{112}Sn is lower than the theoretically predicted one because of the feeding from levels at higher energies. The value of the level at 3435 keV is close to the ratio predicted for a ground state transition indicating its dipole character. One also can see that the angular distribution ratios of all calibration lines of ^{27}Al and ^{13}C are close to 1 as expected for most combinations of semi-integer spins.

4.4 Photon Flux and Integrated Cross Sections

To obtain the final results we used two different methods. The first method becomes possible due to the absolute normalization of the photon flux by measuring simultaneously the well-known excitations in the calibration targets ^{27}Al and ^{13}C. For these calculations we use the relationship between the integrated photon scattering cross section I_S and the properties of the nuclear levels. The peak area A_i of a line in the NRF spectrum can be obtained from

$$A_i = N_{Target} \cdot \int_{T_M} N\left(E_x, E_0, t\right) dt \cdot \varepsilon\left(E_x\right) \cdot I_S^i \cdot W_{eff}^i\left(\theta\right) \cdot \frac{\Delta\Omega}{4\pi}, \tag{4.4}$$

where N_{Target} is the total number of target nuclei irradiated by the incident photons (taking into account the isotopic enrichment), T_M is the total time of measurement, $N\left(E_x, E_0, t\right)$ is the number of photons crossing the unit of target surface per unit of time, $\varepsilon\left(E_x\right)$ is the detector efficiency, $W_{eff}^i\left(\theta\right)$ is the angular distribution function integrated over the solid angle $\Delta\Omega$ of the detector placed at the angle θ, and the E_x is the energy of the excited level.

The number of nuclei in a target is given by

$$N_{Target} = \rho \cdot x \cdot \frac{N_A}{A} \cdot S = \frac{m}{S_{Total}} \cdot \frac{N_A}{A} \cdot S, \tag{4.5}$$

where ρ is the density, x is the target thickness, S equals the area of the target surface irradiated by the photon flux, N_A is Avogadro's number, A is the mass number, m is the target mass and S_{Total} the total target area.

The use of calibration targets with areas equals to the one of allows a direct determination of the product of the photon flux $N_\gamma(E_x, E_0)$ and detector efficiency $\varepsilon(E_x)$. For the $N_\gamma \cdot \varepsilon$ one obtains

$$N_\gamma(E_x, E_0) \cdot \varepsilon(E_x) = \frac{A_i}{N_{Calibr} \cdot I_S^i \cdot W_{eff}^i(\theta) \cdot \frac{\Delta\Omega}{4\pi}}, \tag{4.6}$$

where A_i is the peak area of the i-th calibration ^{27}Al or ^{13}C line. The integrated photon scattering cross sections of the ^{27}Al or ^{13}C lines used for the determination of $N_\gamma \cdot \varepsilon$ are listed in Tab. 4.1. The obtained data of $N_\gamma \cdot \varepsilon$ were fitted with a polynomial

$$N_\gamma \cdot \varepsilon = \frac{a_1}{E} + b_1 + c_1 \cdot E + d_1 \cdot E^2, \tag{4.7}$$

and the result of such a procedure is presented in Fig. 4.7.

The second method is based on the data from the efficiency measurements with ^{56}Co and simulation of N_γ using the Monte-Carlo calculations GEANT. The bremsstrahlung spectrum was simulated [27] using the program GEANT 3.21 with an end-point energy of 3.8 MeV. In Fig. 4.6 the simulated flux fitted with a polynomial function of 5^{th} degree is given. The

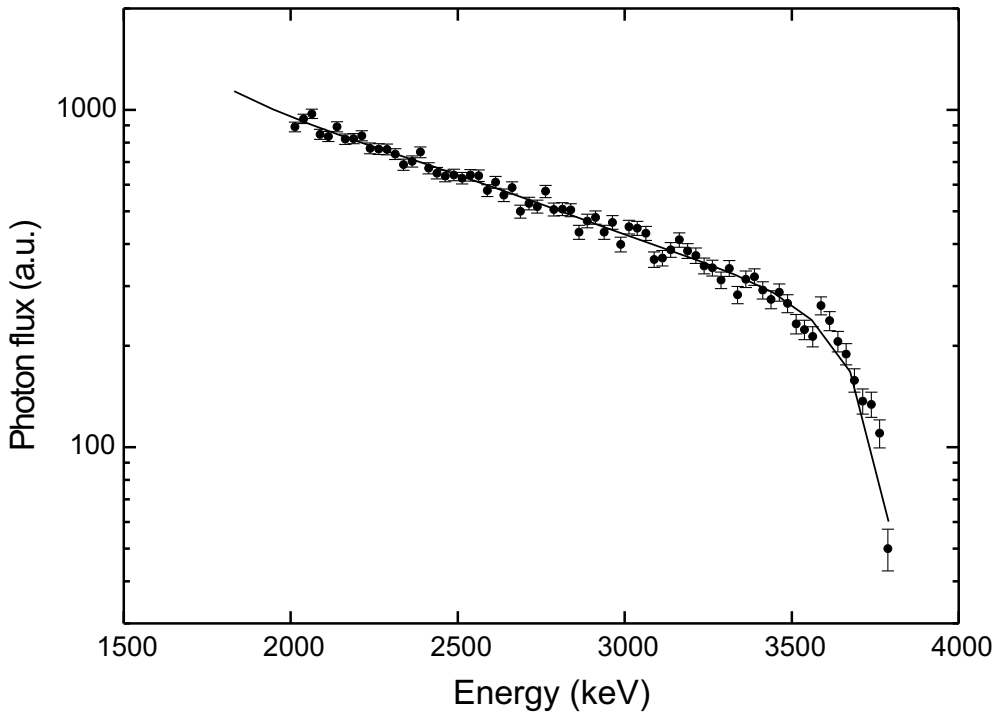

Figure 4.6: Plot of the relative photon flux between 2 and 3.8 MeV. A 5^{th} order polynomial function is applied to fit the shape of the photon flux.

errors are statistical only and are equal to the square root from the number of counts. It is seen that in a broad energy region the photon flux can be represented by a straight line in a logarithmic plot. The absolute normalization of the photon flux cannot be obtained from the simulation in which a much larger opening angle for the emitted bremsstrahlung is accepted than in the experiment [27, 28].

Because GEANT simulations give us only an energy dependence of the flux, but not absolute values we have to normalize these data accordingly to the experimental points of ^{27}Al and ^{13}C. For this procedure one can use a Least

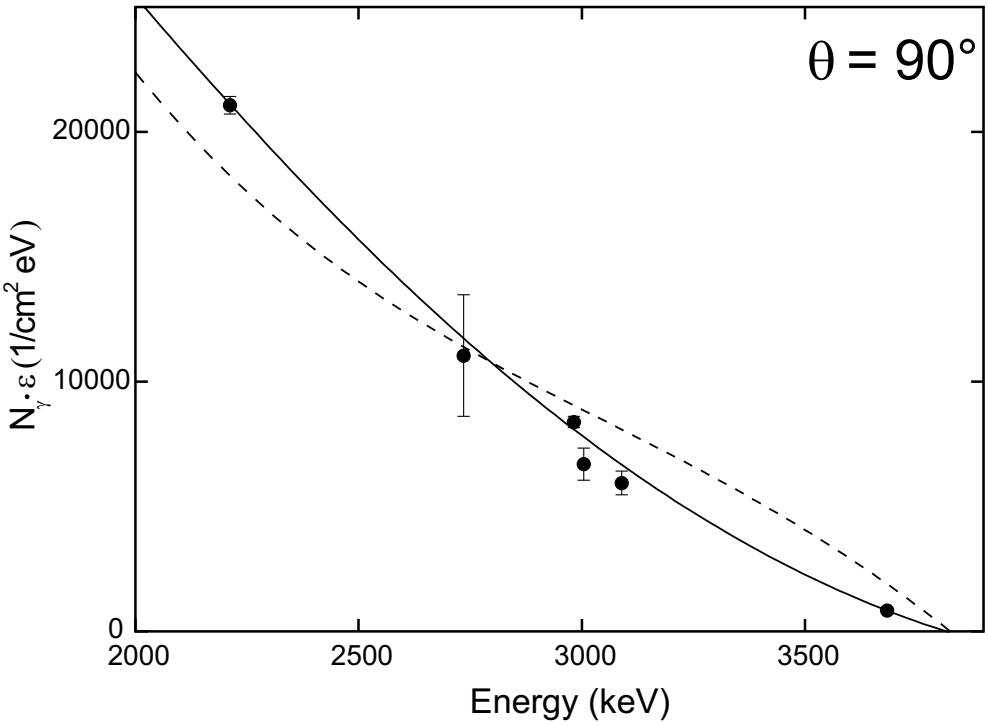

Figure 4.7: Comparison of the $N_\gamma \cdot \varepsilon$ calculated from two different methods. Experimental points are connected by the fit function (solid line), and the Least Squares Fit is presented by a dashed line.

Squares Fit [29].

The comparison of these two methods is presented in the Fig. 4.7. Here the data for ^{27}Al and ^{13}C transitions with error bars are shown as circles, and the solid line is a fit to them with a function representing a product of the measured efficiency and the flux deduced from the GEANT simulations. There is clearly a difference between the predicted energy dependence whose origin of which is presently not understood. Correspondingly, there is a difference in integrated cross section with respect to the result of the transition to the

two-phonon 1^- state. The corresponding values are presented in Tab. 4.3.

Table 4.3: Experimental results of the $^{112}\mathrm{Sn}(\gamma,\gamma')$ reaction at E_0=3.8 MeV.

E_x (keV)	Method	I_S (eV · b)	Γ_0 (meV)	$B(E1)\uparrow$ $\times 10^{-3}$ ($e^2 \cdot fm^2$)
3434.5	Geant and ^{56}Co	119(12)	122(12)	8.6(0.9)
	^{27}Al and ^{13}C	183(19)	187(19)	13.3(1.4)

5 Discussion

In the measured spectra of ^{112}Sn one dipole excitation is observed. The determination of the parity of this state is impossible in the experiment, but the energy is close to the energy of the lowest 1^- states in ^{116,118,120,122,124}Sn isotopes [9, 10]. Therefore, we assume that the state has total angular momentum and parity $J^\pi = 1^-$ and arises due to the coupling of quadrupole and octupole phonons.

From a completely harmonic coupling of the quadrupole and octupole vibrations the excitation energy of the two-phonon multiplet is expected [30] to be the sum of the one-phonon excitation energies $E_x(2^+)$ and $E_x(3^-)$. The experimentally observed excitation energies $E_x(1^-)$ in the tin isotopic chain are lying very close to, but systematically lower than the sum. This nearly perfect correlation between the one-phonon sum energies and the two-phonon energies $E_x(1^-)$ is demonstrated in the Fig. 5.1. The two-phonon anharmonicities are small and result in a minor lowering of the 1^- two-phonon states. The energy ratio $[E_x(1^-)]/[E_x(2^+) + E_x(3^-)]$ is about 93% and constant in the isotopic chain with fluctuations of about 2% as one can see from Tab. 5.1. This ratio was investigated in other nuclei and is approximately equal to 1 with a deviation of 10% in light nuclei [8].

Although the energy of the 1^- state is very close to the sum of the energies of the 2^+ and 3^- states, the only unambiguous identification of this 1^- level as a member of the two-phonon multiplet $(2^+ \otimes 3^-)$ would be a direct measurements of its $E2$ and $E3$ decay transitions into the 3^- and 2^+ one-phonon states. Unfortunately, because of background and transition intensity con-

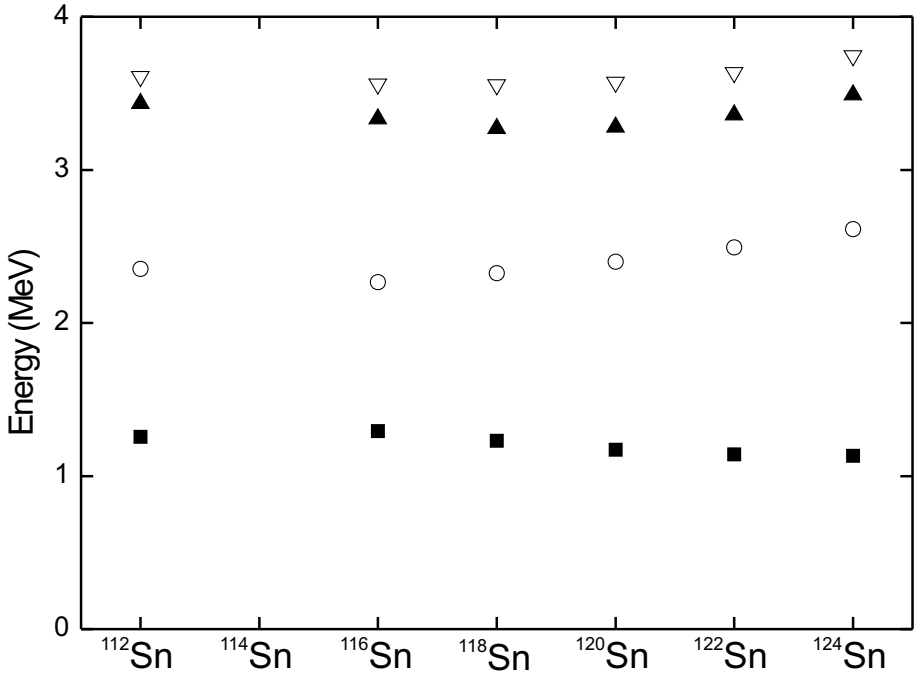

Figure 5.1: Energies of the 2^+ (solid squares), 3^- (open circles) one-phonon states, and the 1^- (solid triangles) two-phonon states in ^{112,116,118,120,122,124}Sn compared to the sum energies $E_x(2^+) + E_x(3^-)$ (open triangles).

siderations, this is not possible in the present photon scattering experiment. But such transitions have been observed in proton scattering experiments at the N = 82 shell closure demonstrating similar transition strengths of the two-phonon to one-phonon decay compared to the one-phonon to g.s. decay [32].

Table 5.1: Propeties of the low-lying 2^+, 3^-, and 1^- levels in the even-even, stable Sn isotopes.

	^{112}Sn	^{116}Sn	^{118}Sn[b]	^{120}Sn[b]	^{122}Sn[b]	^{124}Sn[b]
$E_x(2^+)$[a] (MeV)	1.256	1.294	1.230	1.171	1.141	1.132
$E_x(3^-)$[a] (MeV)	2.354	2.266	2.325	2.401	2.493	2.614
$E_x(1^-)$ (MeV)	3.434[b]	3.334[c]	3.271[c]	3.279[c]	3.359[c]	3.490[c]
$\frac{E_x(1^-)}{E_x(2^+)+E_x(3^-)}$	0.951	0.937	0.920	0.918	0.924	0.932

[a] From Ref. [25].
[b] This work
[c] From Ref. [9].

The values of the $B(E1)$ transition probability in ^{112}Sn extracted with the two different methods are compared in Fig. 5.2 with those for the other ^{116,118,120,122,124}Sn isotopes. The value extracted from the normalization to ^{13}C and ^{27}Al would deviate strongly (about a factor of 2) from the systematics of other isotopes. The result obtained from a normalization to ^{56}Co+GEANT seems to be more likely, but still represents a significant increase with respect to the suggested empirical systematics. The quasiparticle-phonon model (QPM) calculations similar to those for $^{116-124}$Sn are in preparation which can account very well for the observed B(E1) values.

Besides ground state transitions from 1^- there is a probability of decay to the

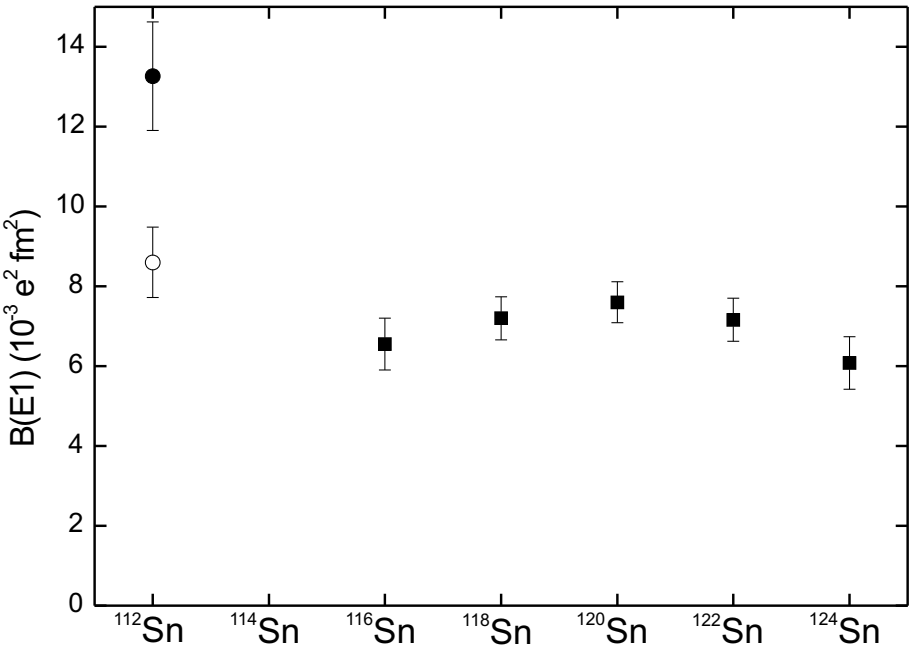

Figure 5.2: Experimental $B(E1)\uparrow$ values for the E1 two-phonon excitations in even-mass Sn isotopes. The $B(E1)\uparrow$ value calculated from the ^{13}C and ^{27}Al transitions is shown as solid circle, and the value from the ^{56}Co efficiency measurements and GEANT simulation as open circle, which are compared to the other even Sn isotopes (see Ref. [9]) with A=116 - 124 (squares).

low-lying states. The decay branching ratio of the photo-excited $J^\pi=1^-$ state to the first $J^\pi=2^+$ state in ^{112}Sn was calculated and was found to be equal to b_1=0.015. This means a very small possibility to observe this transition in the spectra, and also because of the background level in the demanded energy region.

Table 5.2: Known 2^+ levels of ^{112}Sn nucleus below 3.8 MeV.

J_i^π	E_x	E_γ	I_γ
2^+	1256.85	1257.05	100
2^+	2151.09	894.60	100
		2151.00	16.7
2^+	2476.20	1219.30	28
		2475.90	100
2^+	3093.07	1836.50	100
		3092.4	26.2
2^+	3248.81	772.80	25.9
		894.1	27
		3248.1	100
2^+	3286.39	2029.70	84
		3285.6	100

According to the Nuclear Data Sheets the ^{112}Sn isotope has numerous other 2^+ states with an energy below 3.8 MeV (Tab. 5.2). The states at 2151 keV and 3249 keV have a small b_0 branching ratio to the ground state which makes their observation in a (γ, γ') experiment unlikely because of the dependence of I_S on Γ_0^2/Γ, see Eq. (2.12).

For the remaining level, the energy of 2476 keV coincides with a SE line from a ^{27}Al transition, making an observation of the corresponding transition very difficult. For other levels at 3248 keV and 3286 keV the values for the upper limit of the reduced transition probabilities were calculated and they are equal to approximately B(E2) $\simeq 11\ e^2 fm^4$.

6 Conclusion and Outlook

A study of the ^{112}Sn(γ,γ') reaction for energies up to 3.8 MeV was performed at the Stuttgart Dynamitron accelerator. Besides the well-known 2_1^+ state only one transition attributed to ^{112}Sn was found in the spectra. It has dipole character, and it is interpreted as a two-phonon 1^- state because its energy agrees with the systematics established in $^{116-124}$Sn. However the extracted B(E1) strengths deviates strongly from the systematics. Two different methods of the photon flux calibration lead to different results. This discrepancy is presently not understood.

Possible light on this problem can be shed in two ways : there exist real measurements at the ^{112}Sn(γ,γ') reaction at a higher end-point energy performed at the S-DALINAC, which should provide an independent result. Furthermore, QPM calculations similar to the ones performed for $^{116-124}$Sn are in preparation. Those provided very good agreement for the B(E1) transition strengths and could therefore serve as a guide to distinguish which of the two results is correct.

References

[1] P.O. Lipas, Nucl. Phys. **82** (1966) 91

[2] P. Vogel and L. Kochbach, Nucl. Phys. **A176** (1971) 33

[3] M. Grinberg and C. Stoyanov, Nucl. Phys **A573** (1994) 231

[4] F.R. Metzger, *Resonance Fluorescence in Nuclei*, Progr. in Nucl.Phys. **7** (1959) 54

[5] S.J. Skorka, *Nuclear Resonance Fluorescence*, In: The Electromagnetic Interaction in Nuclear Spectroscopy, (W.D.Hamilton, editor), North Holland Publ. Company, Amsterdam (1975) 283

[6] U. Kneissl, H.H.Pitz, and A.Zilges, Prog. Part. Nucl. Phys. **37** (1996)

[7] W. Andrejtscheff, C. Kohstall, P.von Brentano, C. Fransen, U. Kneissl, N. Pietralla, H.H. Pitz, Phys. Lett. **B506** (2001) 239

[8] M. Babilon, T. Hartmann, P. Mohr, K. Vogt, S. Volz and A. Zilges, Phys. Rev. **C65** (2002) 037303

[9] J. Bryssinck, L. Govor, D. Belic, F. Bauwens, O. Beck, P.von Brentano, D.De Frenne, T. Eckert, C. Fransen, K. Govaert, R.-D. Herzberg, E. Jacobs, U. Kneissl, H. Maser, A. Nord, N. Pietralla, H.H. Pitz, V.Yu. Ponomarev and V. Werner, Phys. Rev. **C59** (1999) 1930

[10] J. Bryssinck, L. Govor, V.Yu. Ponomarev, D. Belic, F. Bauwens, O. Beck, P.von Brentano, D.De Frenne, T. Eckert, C. Fransen, K. Go-

vaert, R.-D. Herzberg, E. Jacobs, U. Kneissl, H. Maser, A. Nord, N. Pietralla, H.H. Pitz and V. Werner, Phys. Rev. **C61** (2000) 024309

[11] Nuclear Data Sheets; http://www.nndc.bnl.gov/

[12] H.A. Bethe and G.Placzek, Phys. Rev. **51** (1937) 450

[13] L.W. Fagg and S.S.Hanna, Rev. Mod. Phys. **31** (1959) 711

[14] H. Frauenfelder, R.M. Steffen, *Angular Distribution of Nuclear Radiation in Alpha-, Beta- and Gamma-Ray Spectroscopy*, ed. K.Siegbahn, (North-Holland, Amsterdam, 1965)

[15] J.W. Hammer, H.M. Schnuepferling, E. Bergandt and T. Pflaum, Nucl. Inst. and Meth. **128** (1975) 409

[16] J.W. Hammer, B. Fischer, H. Hollick, H.P. Trautvetter, K.U. Kottner, C. Rolfs and M. Wiescher, Nucl. Inst. and Meth. **161** (1979) 189

[17] H.H. Pitz, U.E.P. Berg, R.D. Heil, U. Kneissl, R. Stock, C. Wesselborg and P.v. Brentano, Nucl. Phys. **A492** (1989) 411

[18] J. Margraf, T. Eckert, M. Rittner, I. Bauske, O. Beck, U. Kneissl, H. Maser, H.H. Pitz, A. Schiller, P.von Brentano, R. Fischer, R.-D. Herzberg, N. Pietralla, A. Zilges and H. Friedrichs, Phys. Rev. **C52** (1995) 2429

[19] B. Schlitt, U. Maier, H. Friedrichs, S. Albers, I. Bauske, P.von Brentano, R.D. Heil, R.-D. Herzberg, U. Kneissl, J. Margraf, H.H. Pitz, C. Wesselborg, A. Zilges, Nucl. Inst. and Meth. Phys. Res. **A337** (1994) 416

[20] H. Maser, S. Lindenstruth, I. Bauske, O. Beck, P.von Brentano, T. Eckert, H. Friedrichs, R.D. Heil, R.-D. Herzberg, A. Jung, U. Kneissl, J. Margraf, N. Pietralla, H.H. Pitz, C. Wesselborg, A. Zilges, Phys. Rev. **C53** (1996) 2749

[21] G.F. Knoll, *Radiation Detection and Measurement*, 2^{nd} Ed. (Wiley, New York, 1989)

[22] P.M. Endt, Nucl. Phys. **A521** (1990) 1

[23] N. Pietralla, P.von Brentano, R.-D. Herzberg, A. Zilges, U. Kneissl, J. Margraf, H. Maser and H.H. Pitz, Phys. Rev. **C52** (1995) R2317

[24] R. Moreh, O. Beck, I. Bauske, W. Geiger, R.D. Heil, U. Kneissl, J. Margraf, H. Maser and H.H. Pitz, Phys. Rev. **C48** (1993) 2625

[25] J.K. Tuli, Nucl. Data Sheets **79** (1996) 725

[26] F. Stedile, Diploma thesis, Universität Stuttgart (1999)

[27] J. Enders, private communication

[28] D. Belic, C. Arlandini, J. Besserer, J.de Boer, J.J. Carroll, J. Enders, T. Hartmann, F. Käppeler, H. Kaiser, U. Kneissl, E. Kolbe, K. Langanke, M. Loewe, H.J. Maier, H. Maser, P. Mohr, P.von Neumann-Cosel, A. Nord, H.H. Pitz, A. Richter, M. Schumann, F.-K. Thielemann, S. Volz and A. Zilges, Phys. Rev. **C65** (2002) 035801

[29] W.R. Leo, *Techniques for Nuclear and Particle Physics Experiments: A How-to Approach*, (Springer-Verlag Berlin Heidelberg, 1994)

[30] J. Enders, P.von Brentano, J. Eberth, R.-D. Herzberg, N. Huxel, H. Lenske, P.von Neumann-Cosel, N. Nicolay, N. Pietralla, H. Prade, J. Reif, A. Richter, C. Schlegel, R. Schwengner, S. Skoda, H.G. Thomas, I. Wiedenhöver, G. Winter and A. Zilges, Nucl. Phys. **A636** (1998) 139

[31] T. Hartmann, J. Enders, P. Mohr, K. Vogt, S. Volz and A. Zilges, Rhys. Rev. Lett. **85** (2000) 274

[32] M. Wilhelm, S. Kasermann, G. Pascovici, E. Radermacher, P.von Brentano and A. Zilges, Phys. Rev. **C57** (1998) 577

[33] M. Babilon, Diploma thesis, TU Darmstadt (2001)

Acknowledgements

At this place I would like to thank all persons who have contributed to the success of this work.

On the first place I would like to sincerely thank *Professor Dr. Dr. h. c. mult. Achim Richter* for the given opportunity to work on such an exciting topic under his supervision and to sense the climate of constructive team work in the modern scientific laboratory.

Further on I would like to thank *Privatdozent Dr. Peter von Neumann-Cosel* for the numerous useful discussions during the realization of this diploma thesis and for valuable remarks that he has made during the reading of this thesis and the significance of which it is difficult to overestimate.

I address my heartfelt gratitude to *Dr. Harald Genz* for his every day help, care and support.

I also would like to thank *Professor Joachim Enders* for numerous discussions during the work.

Furthermore I am grateful to *Professor Dr. Ulrich Kneissl* and *Dr. Heinz-Hermann Pitz* for their help, care and support during the experiment at Stuttgart Dynamitron accelerator.

I would like to express my gratitude also to *Oleksiy Burda, Olena Yevetska, Maksym Miski-Oglu, Natalya Ryezaeyva, Dr. Mykhaylo Gopych* and *Dr. Sergiy Khodyachykh* for their support and numerous significant advices. Thank you very much!

I am also grateful to *Dipl.-Phys. Frank Stedile* and *Dipl.-Phys. Marcus Scheck* for all given information and their help during my work.

I would like to express my gratitude to *E.S. Shmatko, V.D. Afanas'ev, A.F. Shchus* and Chair of the Experimental Nuclear Physics of the Karazin Kharkiv National University (Ukraine) for the time they have spent for my education.

I also grateful to *Maksym Chernykh* for care and support during my staying in Germany. Thank you very much!

Finally, my heartful gratitude to my family - my parents *Sergiy* and *Larysa* and my brother *Artem*, and to my friends in Ukraine. Your thoughts and your care were supporting me very much during my study in the Karazin Kharkov University and during my stay in Darmstadt.